Microtubule plus-end conformations and dynamics in the periphery of interphase mouse fibroblasts

Zovko, S.; Abrahams, J.P.; Koster, A.J.; Galjart, N.; Mommaas, A.M.

Molecular Biology of the Cell
Vol. 19, 3138–3146, July 2008

Microtubule Plus-End Conformations and Dynamics in the Periphery of Interphase Mouse Fibroblasts

Sandra Zovko,* Jan Pieter Abrahams,† Abraham J. Koster,* Niels Galjart,‡ and A. Mieke Mommaas*

*Section Electron Microscopy, Department of Molecular Cell Biology, Leiden University Medical Center, 2300 RC, Leiden, The Netherlands; †Department of Biophysical Structural Chemistry, Leiden Institute of Chemistry, Gorlaeus Laboratories, Leiden University, 2300 RA Leiden, The Netherlands; ‡Department of Cell Biology and Genetics, Erasmus Medical Center, 3000 DR Rotterdam, The Netherlands

Submitted August 15, 2007; Revised April 21, 2008; Accepted May 2, 2008
Monitoring Editor: Erika L. Holzbaur

The plus ends of microtubules (MTs) alternate between phases of growth, pause, and shrinkage, a process called "dynamic instability." Cryo-EM of in vitro–assembled MTs indicates that the dynamic state of the plus end corresponds with a particular MT plus-end conformation. Frayed ("ram's horn like"), blunt, and sheet conformations are associated with shrinking, pausing, and elongating plus ends, respectively. A number of new conformations have recently been found in situ but their dynamic states remained to be confirmed. Here, we investigated the dynamics of MT plus ends in the peripheral area of interphase mouse fibroblasts (3T3s) using electron microscopical and tomographical analysis of cryo-fixed, freeze-substituted, and flat-embedded sections. We identified nine morphologically distinct plus-end conformations. The frequency of these conformations correlates with their proximity to the cell border, indicating that the dynamic status of a plus end is influenced by features present in the periphery. Shifting dynamic instability toward depolymerization with nocodazole enabled us to address the dynamic status of these conformations. We suggest a new transition path from growth to shrinkage via the so-called sheet-frayed and flared ends, and we present a kinetic model that describes the chronology of events taking place in nocodazole-induced MT depolymerization.

INTRODUCTION

The microtubule (MT) network forms a major component of the cytoskeleton of the eukaryotic cell. MTs are involved in a number of vital cellular processes, including cell division, cell motility, general cell morphology, and cargo transport. MTs are hollow ~25-nm-diameter tubes assembled from α/β-tubulin heterodimers, which are organized in a head-to-tail manner in protofilaments that laterally interact with each other (Mandelkow and Mandelkow, 1985). The plus end, exposing the β-tubulin subunits, is dynamically unstable and oscillates between phases of relatively slow growth, pausing, and rapid shrinkage. The switch from growth to shrinkage is termed "catastrophe," and the switch from shrinkage to growth "rescue." The minus end, exposing the α-tubulin subunits, is less dynamic (Mitchison and Kirschner, 1984; Mitchison, 1993). In many cell types the MT minus end is embedded in the MT-organizing center (MTOC).

Both tubulin subunits bind GTP (Caplow and Reid, 1985) but only the β-subunit hydrolyzes GTP. MTs elongate by the addition of GTP-bound tubulin subunits or small oligomers at the MT plus end (Kerssemakers *et al.,* 2006). Longitudinal contacts within the MT lattice stimulate the β-subunits of polymerized tubulin to hydrolyze GTP. The crucial feature behind dynamic instability is thought to be the difference in structure between the GTP-tubulin heterodimer and GDP-tubulin heterodimer: the first is relatively straight, whereas the GDP-tubulin heterodimer exhibits a curved conformation (Caplow, 1992; Ravelli *et al.,* 2004; Krebs *et al.,* 2005; Nogales and Wang, 2006). As the GDP-dimers in the protofilaments of the MT are forced to stay straight by lateral contacts, the energy of the curvature is stored within the lattice in the form of tension, making MTs unstable and easy to depolymerize (Caplow *et al.,* 1994) .When the GTP cap at the end of a MT is lost, protofilaments can adopt a curved conformation, resulting in the weakening of lateral interactions between the protofilaments and causing a catastrophe and collapse of the MT (Caplow *et al.,* 1994; Janosi *et al.,* 2002; Nogales and Wang, 2006).

Cryo-electron microscopy (cryo-EM) studies of in vitro–assembled or extracted MTs indicated that the phases of shrinkage, pausing, and growth might correspond to specific structures at the plus end. These are called frayed (coiled, "ram's horn"), blunt and extended (straight, tapered, sheet-like), respectively (Mandelkow *et al.,* 1991; Chrétien *et al.,* 1995; Arnal *et al.,* 2000). In the elongation phase, as the GTP-tubulin dimers and/or small oligomers are added at the plus end, a two-dimensional (2D) sheet is formed that gradually closes in a zipper-like manner (Chrétien *et al.,* 1995; Wang and Nogales, 2005; Kerssemakers *et al.,* 2006; Nogales and Wang, 2006). The sheet can close to form a tube, thereby adopting the blunt-end conformation (Chré-

This article was published online ahead of print in *MBC in Press* (http://www.molbiolcell.org/cgi/doi/10.1091/mbc.E07–07–0681) on May 14, 2008.

Address correspondence to: Sandra Zovko (zovko.sandra@gmail.com).

Abbreviations used: EB1, end binding protein 1; EM, electron microscopy; ET, electron tomography; GDP, guanosine 5′-diphosphate; GTP, guanosine 5′-triphosphate; kMT, kinetochore microtubule; LM, light microscopy; MT, microtubule; +TIPS, plus-end tracking proteins.

tien *et al.*, 1995; Arnal *et al.*, 2000), which was suggested to be a metastable transition state between growth and shrinkage (Tran *et al.*, 1997; Arnal *et al.*, 2000; Janosi *et al.*, 2002). Loss of the GTP cap triggers curving of the protofilaments (i.e., GTP-tubulin becomes GDP-tubulin, which has a relatively curved conformation), which then peel off outward from the MT axis (frayed end).

Insight into MT dynamic instability and the factors influencing it in vivo is essential for understanding the nature of malfunction of MT dynamics in diseased cells. In vivo, MT dynamics are regulated by a variety of cellular factors (Lieuvin *et al.*, 1994; Saoudi *et al.*, 1998; Perez *et al.*, 1999; Schuyler *et al.*, 2001; Kovacs and Csaba, 2005; Lansbergen and Akhmanova, 2006). Furthermore, MTs in vivo predominantly have 13 protofilaments, whereas MTs assembled in vitro are made of either 13 or 14 protofilaments. These structural differences seem to be reflected by the plus end of MTs in vivo. In recent years, studies of kinetochore MT (kMT) plus ends in *Caenorhabditis elegans* (O'Toole *et al.*, 2003), plant cells (Austin *et al.*, 2005), PtK_1 and *Drosophila* cells (VandenBeldt *et al.*, 2006; Maiato *et al.*, 2006), and in yeast (Höög *et al.*, 2007) not only confirmed the existence of the plus-end conformations observed in vitro but also introduced a number of new conformations. Not all of the newly introduced forms were found in each of these studies and their dynamic states remained unknown.

To gain more insight into MT dynamic instability in vivo, we studied MT plus ends of interphase mouse 3T3 fibroblasts using EM, electron tomography (ET), and fluorescence microscopy. We focused on MT plus ends in the very periphery of these cells, for it is known that dynamic instability is enhanced at the cell membrane (Komarova *et al.*, 2002; Vorobjev *et al.*, 2003). To correlate a particular MT plus-end conformation to its dynamic state, we studied depolymerization kinetics using nocodazole. Furthermore, we quantified the distribution of plus-end conformations over two zones within the cell periphery. On the basis of our results, we propose a kinetic model that integrates the dynamic state of MT plus ends with their conformation.

MATERIALS AND METHODS

Cell Culture

Mouse 3T3 fibroblasts were cultured in DMEM, supplemented with 10% fetal bovine serum, 2 mM L-glutamine, and antibiotics, in a humidified atmosphere with 5% CO_2 at 37°C.

Specimen Preparation for EM

3T3 cells were grown on 13-mm-diameter Thermanox (Nunc, Naperville, IL) coverslips for 2 d (70% confluence). The cells were cryo-fixed by plunge-freezing the coverslips in liquid ethane in an automated system with a temperature- and humidity-controlled chamber. The atmosphere in the chamber was humid and had a temperature of 37°C. It took 10 s between putting the coverslip with cells into the chamber and plunging it, whereas vitrification was instantaneous upon plunging.

Cryo-immobilized samples were then subjected to freeze-substitution in a mixture of 0.01% OsO_4 and 0.25% uranyl acetate in absolute acetone. Freeze-substitution was performed in Automatic Freeze Substitution apparatus (AFS, Leica, Deerfield, IL) for 72 h at −90°C. The temperature was then gradually raised (10°/h) to −20°C and maintained at this temperature for 12 h. Afterward, the temperature was raised to 0°C (10°/h).

Subsequently, cells were washed twice for 15 min with acetone. The specimens were then infiltrated with epoxy resin and flat-embedded. Sections of 100–150 nm were made parallel to the cell attachment plane. The samples were poststained with uranyl acetate and a lead–salt mixture for 15 and 5 min, respectively.

EM and Electron Tomography

Thin sections were analyzed using a CM-10 Transmission Electron Microscope with a LaB6 filament operating at 80 kV.

For quantitative analysis, various plus ends in the area of maximally 5 μm from the plasma membrane toward the cell interior were scored and categorized. In total 164 plus ends were scored. Projection of a MT shows two dark lines caused by the superposition of protofilaments in the direction of projection (i.e., the "sides" of the MT), having a higher signal than the "bottom" and "top" of the MT. Classification was based on the degree of line curvature and on the difference in line length at the plus end of the MT. False positives (MT cut gratingly) were filtered out.

3D tomograms were collected on previously classified MT plus ends in order to verify the classification based on 2D images. Using Inspect 3D (FEI, Beaverton, OR) software, tomographic series of MT plus ends were collected, performing single-axis tilt series from −60 to +60° with increments of 1° in a Tecnai-12 (FEI)equipped with a LaB6 filament operating at 120 kV. 2kx2k binned images were recorded in focus using a CCD camera (4k Eagle) at a magnification of 30,000×. Tomographic tilt series were analyzed and processed using IMOD (Colorado University, Boulder). Projection images were preprocessed by hot pixel removal and roughly aligned by cross-correlation. Final alignment was performed using 10-nm colloidal gold as fiducial markers (Ress *et al.*, 1999). Tomograms were obtained using weighted back-projection.

To establish the potential correlation between plus-end conformations and their location within the cell, the cell periphery was divided into two zones, either 0–2 μm or 2–5 μm away from the cell border. In zone 0–2 μm 51 MT plus ends and in the zone 2–5 μm 113 MT plus ends could be classified.

Kinetic Analysis of MT Depolymerization by Nocodazole in 3T3 Cells

For the MT shrinkage-induction experiments cells were exposed to 10 μM nocodazole (dissolved in culture medium) for 5, 30, 60, or 120 s before blotting and subsequent freezing. Because there is a 10-s delay between blotting and vitrification (which stops depolymerization), the total exposure times to nocodazole were 15, 40, 70, and 130 s, respectively. The experiment was replicated three times for each time point. During the exposure to nocodazole, the cells were kept at 37°C in a humidified atmosphere with 5% CO_2. Cryo-fixation and freeze-substitution followed by flat embedding were performed as described above.

We analyzed 451 MT plus ends in nocodazole-treated cells in total using EM as described above.

For the analysis of the nocodazole time series, the frequency distribution of plus-end states of unexposed cells was used as the starting situation at (t = 0 s). At every time point, mean percentages of the various conformations of plus ends (together with their SDs) were calculated from these triplicates as follows:

$$\sigma_t = \sqrt{((\Sigma(f_{o,t} - f_{m,t})^2)/(N - 1))}$$

where σ_t is the standard deviation at time t, $f_{o,t}$ is the observed frequency at time t, $f_{m,t}$ is the mean frequency at time t, and N is 3 (every experiment was performed in triplicate). Two conformations (sheet-straight and sheet-frayed 1) were not observed at t = 130 s, and at these two points the SD was assumed to be equal to $\sqrt{2/3}$ times the expected frequency.

Scoring Plus Ends by Fluorescence Microscopy

3T3 fibroblasts were grown overnight to ~40% of confluence on glass coverslips, before cryo-fixation (see above) and freeze-substitution in pure acetone without additional fixatives. When a temperature of −20°C was reached, samples were fixed with methanol/EGTA for 12 min. Subsequently, cells were washed with phosphate-buffered saline (PBS) and incubated in blocking buffer for 45 min at room temperature. Cells were incubated for 1 h at room temperature with primary antibodies against tyrosinated tubulin (rat monoclonal, clone YL1/2, Abcam, Cambridge, MA), diluted in blocking buffer, and against a marker of the plus ends of growing MTs (EB1, mouse monoclonal, Transduction Laboratories, Lexington, KY), diluted in blocking buffer. The samples were washed three times for 15 min in PBS/0.05% Tween-20 and incubated with goat anti-rat Alexa488 and goat anti-mouse Alexa594 secondary antibody (both Molecular Probes, Eugene, OR) for 1 h at RT. Next, cells were washed three times in PBS/0.05% Tween-20, and in 70 and 100% ethanol, air-dried, and mounted on a glass slide using Vectashield mounting medium (Vector Laboratories, Burlingame, CA) with DAPI nuclear staining.

Immunofluorescent images were collected using a Leica DMRXA microscope with a CoolSnap K4 camera using ColorPro software (Roper Scientific, Tucson, AZ). MT plus ends, stained for EB1 or tubulin, were scored in the cytoplasm up to ~5 μm from the cell border. Only areas of the cell where MTs were sparse enough to distinguish them separately were used for analysis.

The fluorescence microscopy images were processed with Photoshop (Adobe, San Jose, CA). The area of interest (~5 μm from the cell border inward) was marked. To improve visibility of the MT contrast, an emboss filter was applied (0 and 90°). Next, the MTs were manually tracked and marked at both 0 and 90° embossed images in two different colors. The two images were then superimposed, resulting in good visibility of the MTs in the images. The superimposed image revealed the spatial position of the MTs in

the cell periphery, enabling scoring of the total number of MTs and MT plus ends.

RESULTS

Nine Distinct Plus-End Conformations in the Periphery of Interphase 3T3 Cells

To produce a sample in which we could trace MTs, and therefore reliably locate MT plus ends, several experimental procedures were introduced. First, we used Thermanox coverslips instead of glass, because the latter break upon Epon capsule removal. 3T3 cells grown on Thermanox coverslips were flat and spread out properly allowing easy cryo-vitrification of the sample. Flat-embedded cells could then be sectioned in the plane of cell attachment, ensuring sample sections largely parallel to the MT network. As 3T3 cells have a relatively large and flat periphery, the MT network could be studied in a single thin plane, often 200–100-nm thick (Figure 1A).

We selected and categorized MT ends that pointed toward the cell membrane, because these are predominantly MT plus ends rather than minus ends (Figure 1, B and C). Electron tomography enabled us to extract 3D representations of the plus ends inside the tomographic volume. This allowed further 3D characterization of the various plus-end features and permitted relating these to their projection images.

Taking distinct morphological characteristics of MT plus ends into account (see *Material and Methods* and Wade and Chrétien, 1993), we were able to classify them into nine groups. Example projection images and tomographic slices of the nine MT plus-end conformations are shown in Figure 1, D–F. The early-frayed and frayed ends are characterized by the ram's horns conformation (Mandelkow and Mandelkow, 1985), i.e., the protofilaments at both sides of the MT end curve away to a similar extent from the MT axis. The early-frayed end is characterized by relatively short tips of protofilaments bending away from the MT axis (VandenBeldt *et al.*, 2006), whereas in the frayed-end protofilaments curve away further, resulting in protofilament coils. The degree of projected protofilament curvature was defined as the angle between the MT wall and the straight line drawn from the point the bending started to the tip of the curved protofilament. In the early-frayed end this angle ranged from 19 to 45° with an average angle of 35 ± 10°. In the frayed end the curvature angle ranged from 54 to 180° with average angle of 106 ± 31°.

MT ends of the forked conformation are directed away from the MT axis, but they are straight rather than curved. In projection, this outward redirection of straight protofilaments appears to introduce a "break" or "kink" in the MT lattice. The protofilaments in the forked end terminate more or less simultaneously. By contrast, in the sheet-frayed 2 end, we observed the protofilaments to curve away from the MT axis at different heights. In the sheet-frayed 2 plus end, the curvature of protofilaments pointing away from the lattice was similar to that of the early-frayed and frayed ends.

The sheet-straight conformation has straight ends of unequal length. Thus, the straight-sheet resembles sheet-frayed 2 except that the latter has curving protofilaments, as in (early)-frayed plus ends. The sheet length (distance between the protofilament ends at the "long" and "short" sides of the

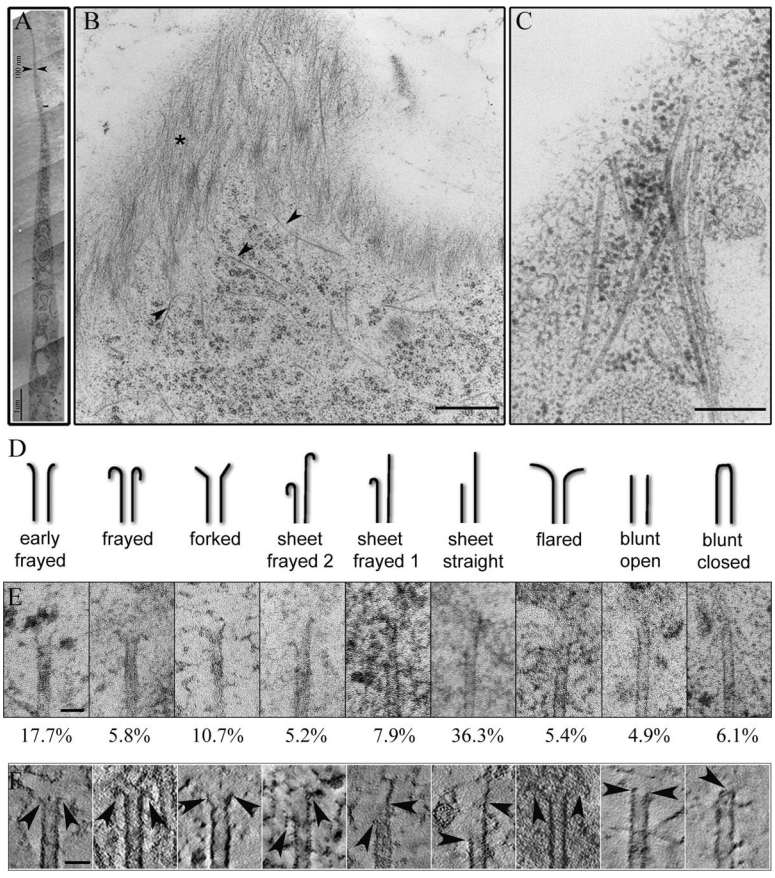

Figure 1. Nine distinct plus-end conformations in the periphery of the 3T3 cells. (A) Ten stitched micrographs showing the side view (section perpendicular to cell attachment plane) of the periphery of a sectioned cryo-fixed, freeze-substituted, and flat-embedded 3T3 cell. The cells become as thin as 80 nm at the cell periphery (thickness indicated by the two arrows is 100 nm). Bar, 1 μm. (B) Periphery of a 3T3 cell, sectioned parallel to its attachment plane, with MTs running toward the cell membrane (arrows) and cortical actin filaments (asterisk). Bar, 0.5 μm. (C) MT plus ends in proximity of the cell border. Bar, 0.3 μm. (D) Cartoon of MT plus-end conformations found in the periphery of the 3T3 cells with class annotation below each image. From left to right: early-frayed, frayed, forked, sheet-frayed 2 and 1, sheet-straight, flared, blunt-open, and blunt-closed conformations. (E) Electron micrographs of the nine plus-end conformations corresponding to the diagrams in D. The percentages underneath the micrographs stand for the frequency of a particular plus-end conformation in control 3T3 cells. Bar, 50 nm. (F) Tomographical slices, 5-nm thickness, of plus-end conformations shown in the same order as in D and E. Arrows point to the plus-end tips. Bar, 50 nm.

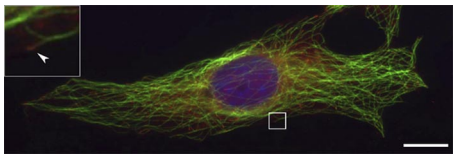

Figure 2. Fluorescent microscopy image of a cryo-vitrified, freeze-substituted, and subsequently fluorescently stained 3T3 cell with MTs in green, EB1 in red, and nucleus in blue. MTs often extend from the area around nucleus toward the cell border. MT plus ends labeled with EB1 are in the growth phase (arrowhead in the top left panel). Counting the MT plus ends (total) and EB1-labeled plus ends, a fraction of growing plus ends was assessed. Bar, 10 μm.

lattice) was found to range from 50 to 320 nm (n = 29, with mean 105 ± 62 nm), i.e., ~6–40 tubulin subunits. This is in the same range as the length reported by Austin *et al.* (2005) for sheet ends in plant cells (50–300 nm).

The sheet-frayed 1 conformation is a combination of sheet-straight and sheet-frayed 2 ends as it has both a straight extension and a curved part. The flared end has long, smoothly curving protofilaments extending away from the MT axis. Similar to forked ends, flared ends have a funnel-like shape, and sometimes it was difficult to distinguish between forked and flared ends. However, the straight protofilaments typical for forked are not present in flared ends. Flared ends have been observed previously by others (see also first image on the left in Figure 2C in Mandelkow *et al.*, 1991).

Finally, we classified blunt-open and blunt-closed ends. In the first the protofilaments are straight and terminate more or less simultaneously. In the blunt-closed end we observe a rounded, cap-like structure at the very tip of the MT.

Next we analyzed the frequency of each plus-end conformation in the cell periphery, extending maximally 5 μm from the cell membrane toward the interior (Figure 1E, frequencies are shown in percentage below the different panels). Out of a total of 164 plus ends, most ends (36.3%) were found to exhibit a sheet-straight conformation. The second-largest fraction is formed by the early-frayed ends (~18%). Forked ends (~11%) and sheet-frayed 1 ends (~8%) are present in intermediate amounts, whereas the frayed ends (~6%), sheet-frayed 2 ends (~5%), flared ends (~5%), and blunt-open and blunt-closed ends (together ~11%) are present in lower numbers (Figure 1E).

Half of the Plus Ends in the 3T3 Periphery Are Decorated by EB1

The growing plus ends of MTs are easily distinguished in fluorescence microscopy with antibodies against plus-end binding proteins (+TIPs), such as EB1 (Stepanova *et al.*, 2003). We estimated the fraction of plus ends of growing MTs in the periphery of the 3T3 cells by immunolabeling MTs and their growing plus ends with antibodies against tubulin and EB1, respectively (Figure 2). We ensured that the results obtained by fluorescence microscopy could be correlated with our EM data (see *Material and Methods*). We analyzed the total amount of MT plus ends and plus ends of growing MTs in an area that was maximally 5 μm from the cell membrane. We analyzed six representative cells and found that the mean percentage of EB1-labeled MT plus ends was 53.7 ± 19.5% (in total 686 MT plus ends counted, ±115 per cell), indicating that half of the MTs in the periphery of the cell were growing.

Nocodazole Affects the Distribution of Plus-End Conformations

To correlate the MT plus-end conformation to the actual dynamic state of a MT, we shifted the balance of dynamic instability toward shrinkage by exposing cells to nocodazole. Nocodazole binds free GTP-tubulin, which can no longer be incorporated into MTs. Thus, nocodazole inhibits MT growth and therefore induces MT dissociation. This MT dissociation is a first-order reaction because it is independent of the concentration of free tubulin, as nocodazole prevents the latter from reassociating. After 130 s of nocodazole treatment, MTs were still present in the periphery of the cells, as observed with light microscopy (LM) of fluorescently labeled MTs (Supplemental Figure S1).

Next we examined the periphery of nocodazole-treated cells by EM. We analyzed in total 451 MT plus ends in nocodazole-treated cells. We observed that the fractions of the various conformations of plus ends altered as a function of the duration of exposure to nocodazole (Figure 3, A–H, measured values given by filled squares). The adjunct values are given in Supplemental Table S1.

Nocodazole clearly causes a significant shift toward the generation of frayed ends, i.e., MT ends with ram's horns. After 130 s of exposure ~80% of the plus ends exhibited a frayed conformation (Figure 3A). We observed an increase of sheet-frayed 1 upon 15 and 40 s of nocodazole exposure, followed by a decrease as the treatment continued (Figure 3B). A similar trend was observed for sheet-frayed 2 ends, yet here the increase peaked at a later time point, i.e., after 70 s of nocodazole exposure (Figure 3C). Flared-end frequency increased after 15 and 40 s of nocodazole exposure, to go down to the basic levels after 70 s of exposure (Figure 3D). By contrast, the frequency of early-frayed ends decreased from 17 to 9% in the first 15 s of exposure to nocodazole, to remain relatively constant after prolonged exposure (Figure 3E). Nocodazole treatment also affected the frequencies of sheet-straight ends and forked ends, which dropped from 36 to 0% for the sheet-straight and from 11 to 4% for the forked ends after nocodazole exposure for 130 s (Figure 3, F and G, respectively). The blunt-open frequency also decreased upon exposure to nocodazole (Figure 3H). Finally, blunt-closed ends disappeared already after 15 s of nocodazole exposure, suggesting that if the blunt-closed form represents a MT minus end, nocodazole also influences the minus-end cap.

To characterize the kinetics of MT depolymerization, we determined the set of rate equations that best explained our observed data. We fitted a set of eight differential equations with 56 unknown rate constants to the kinetic experimental data (lines in the graphs shown in Figure 3, A–H). Each of the eight differential equations had the following form:

$$\delta[M_a]/\delta t = k_{ba}[M_b] + k_{ca}[M_c] + k_{da}[M_d] + k_{ea}[M_e] + k_{fa}[M_f] + k_{ga}[M_g] + k_{ha}[M_h] - (k_{ab} + k_{ac} + k_{ad} + k_{ae} + k_{af} + k_{ag} + k_{ah})[M_a]$$

where k_{xy} is the rate constant of the transition of M_x into M_y and $[M_a]$ to $[M_h]$ are the observed frequencies at a given time point of each of the types of microtubule ends (either early-frayed, frayed, forked, sheet-frayed 1, sheet-frayed 2, sheet-straight, flared, and open blunt). We did not include the blunt-closed ends in our analysis because previous studies suggested this conformation to be a MT minus end (O'Toole *et al.*, 2003) and because this plus-end conformation was not observed in the presence of nocodazole.

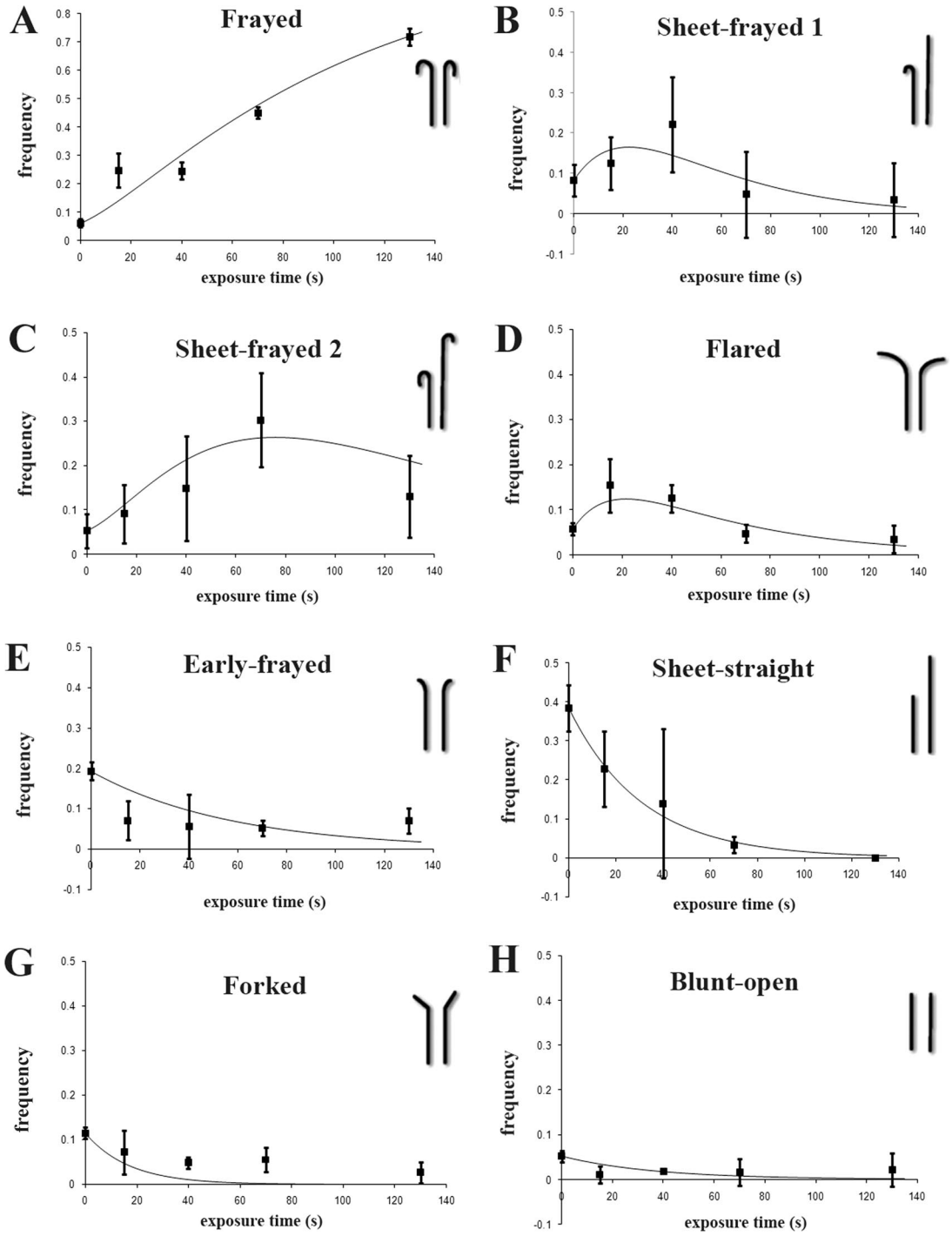

Figure 3. Nocodazole alters the ratios of plus-end conformations in 3T3 cells. 3T3 cells were exposed to 10 μM nocodazole for 0, 15, 40, 70, and 130 s. We scored various plus-end conformations in the area 0–5 μm from the cell border into the cell center for each time point. The measured values are represented by filled squares. We fitted the kinetic data (black curves in the graphs) to a set of linear differential equations by minimizing the χ^2 value between the predicted and observed frequencies. Nocodazole clearly caused a significant shift toward generation of frayed ends (A) and loss of sheet-straight ends (F). The frequency of the sheet-frayed 1 and 2 ends increased during the first 40 and 70 s, respectively, to decrease again after prolonged exposure to nocodazole (B and C). The same trend was observed for flared ends; however, the peak frequency for these ends was reached at t = 15 s (D). Nocodazole induced a decrease of frequency of the early-frayed (E), forked (G), and open-blunt ends (H). Note the larger scale used in A. For the numerical representation of these data see Table 1 and Supplemental Material.

Subsequently, the fit—as defined by the χ^2 statistic—between the calculated kinetic model and the observed, experimental kinetic data was optimized using the standard simplex minimization procedure implemented in the GNU Scientific Library (GSL). We implemented an algorithm based on simplex minimization that allows all rate constants

to vary independently and that converges on a combination of rate constants that correspond to a maximum of the χ^2 statistic. In order not to bias the result to any presupposed mechanism, we initially allowed all interchanges between all the different plus-end conformations, even very unlikely transitions (e.g., sheet-frayed 1 into sheet-straight). In order not to bias the result to the initial values assigned to the rate constants at the start of the fitting procedure, we repeated the analysis, starting with many different (combinations of) initial rate constants. In all cases, most of the rate constants converged to zero within a few cycles of minimization, indicating that the corresponding transitions were forbidden by any kinetic model. When rate constants vanished in this manner, we fixed them to zero, effectively prohibiting the corresponding transition in subsequent refinement steps. Fitting procedures starting from many different combinations of rate constants all converged to just a few potential models and from these models we selected the one with the highest similarity between interchanging plus ends. The most probable model is a compromise between the precision of the fit and the number of kinetic rate constants that are needed to explain the data. The χ^2 statistic allowed us to calculate the kinetic model with the highest probability (i.e., the best fit with the least number of kinetic rate constants). For the forked plus end, this procedure resulted in an apparently suboptimal fit, with most data points above the curve. However, as a result of this particular suboptimal fit, the other kinetic curves could be fitted much more accurately. The most likely kinetic model had seven free parameters (the seven rate constants we report here) and 40 observed restraints with SDs, and its χ^2 statistic was 15.11, indicating a Q-value (or probability that the result was not obtained by chance fluctuations) of 0.997. This kinetic model conformed in general terms to existing models of microtubule depolymerization.

According to our kinetic analysis three types of transition can occur upon nocodazole exposure (Figure 4). In the first (Figure 4, vertically arranged set of transition reactions), the sheet-straight end transforms into the sheet-frayed 1 end (rate constant is 0.03 s^{-1}), and this end transforms into the sheet-frayed 2 end (rate constant is 0.04 s^{-1}). The sheet-frayed 2 end subsequently transforms into a frayed end (rate constant is 0.02 s^{-1}). A second transition path leads from the forked and early-frayed end toward the frayed end (Figure 4, left hand set of reactions). Here, the forked and early-frayed ends transform into a flared end (rate constant are 0.06 and 0.02 s^{-1}, respectively), and a flared end subsequently converts into a frayed end (rate constant is 0.03 s^{-1}). Finally, a blunt-open end can also transform into a frayed end (rate constant is 0.03 s^{-1}) without any intermediate form (Figure 4, right-hand reaction). The kinetic analysis suggests that sheet-straight, blunt-open, and (at least a fraction) of forked and early-frayed ends is likely to represent the growing states of MT plus ends, whereas the frayed ends are confirmed to represent the shrinking ends. Flared and sheet-frayed 1 and 2 might represent transition states originating from growing MT plus ends that have undergone catastrophe.

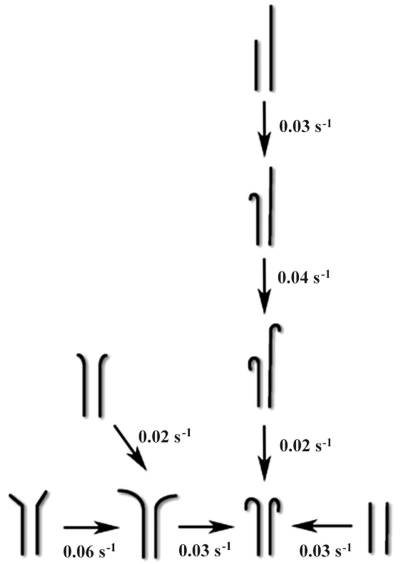

Figure 4. Transformation path model for in vivo microtubule plus-end conformations. Arrows stand for transitions between the dynamic plus-end states estimated by kinetic analysis after exposing cells to nocodazole. Calculated rate constants are given for each transition. According to our analysis, upon nocodazole treatment a plus end with a sheet-straight conformation transforms into a sheet-frayed 1, which upon prolonged nocodazole exposure transforms into sheet-frayed 2, switching eventually into a frayed end (vertical path). Another path starts with a forked end that transits into a frayed end via flared conformation (horizontal path). Similarly to a forked conformation, early-frayed transits into a frayed end via flared conformation. A blunt-open end directly transits into a frayed end upon nocodazole-induced disassembly.

The Cell Periphery Affects Plus-End Conformations

In the cell interior MTs grow (or shrink) persistently, whereas close to the membrane an oscillatory behavior is observed, with individual MTs frequently switching between phases of growth, pause, and shrinkage (Komarova *et al.,* 2002). According to our data at dynamic equilibrium, 34% of the population of the MTs in the searched area (0–5 μm from the cell periphery) was associated with shrinking ends (frayed, early-frayed, flared, and sheet-frayed 2 together), whereas 52% of MTs was associated with stable and/or growing ends (forked, blunt-open, and sheet-straight together). The latter number is in close agreement with our immunofluorescence data using antibodies against EB1. Thus, using EM methods we detect 1.5 times more conformations associated with growing plus ends than shrinking ones.

To test whether the cell periphery affects MT plus-end conformation, we examined if there is a correlation between plus-end conformation and spatial distribution within the peripheral area of the cell. In a zone that was 0–2 μm from the cell membrane we measured the conformation of 51 MT plus ends and in a zone of 2–5 μm from the membrane we measured 113 MT plus ends. Figure 5 shows the distribution of plus ends per class and per zone. The adjunct values are given in Supplemental Table S2. The frequency of frayed, sheet-frayed 2 and flared ends was higher in the zone closest to the membrane (each ~15–17 vs. 0.5–1%, respectively). By contrast, the sheet-straight and blunt-open ends were much less frequent near the cell edge (12 and 2%, respectively, in 0- 2 μm zone, vs. 47 and 6% in 2–5 μm zone). Early-frayed, forked, sheet-frayed 1, and blunt-closed ends were more or less evenly distributed. In the 0–2-μm zone, 45% of the plus ends have conformations associated with shrinkage (frayed, sheet-frayed 2, and flared ends), whereas the typical growth-associated conformations (forked, sheet-straight, and blunt open) make ~24%. Furthermore, in the zone 2–5 μm the growth-associated conformations are dominant over the shrinkage-associated conformations (Figure 5). Combined the data show that the features present in the cell periphery do affect MT plus-end conformation.

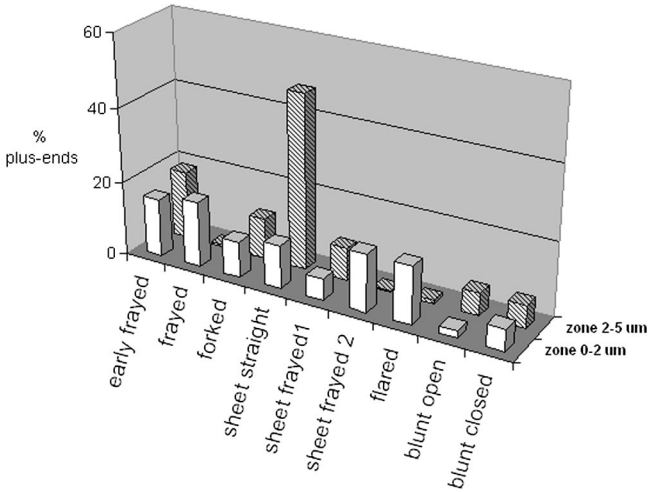

Figure 5. Effect of proximity of the cell border on the distribution of the plus-end conformations in the cell periphery. Periphery of the 3T3 cell was divided in two zones from the cell border toward the cell interior, zone 0–2 μm and 2–5 μm from the cell border (with cell border at the position 0 μm). In the zone 0–2 μm and in the zone 2–5 μm, respectively, 51 and 113 MT plus ends were counted. The values were normalized for total number MTs per zone. In the zone 0–2 μm (□) (early) frayed, sheet-frayed 2, and flared plus ends were most prominent (each ~16–17%). Except for early-frayed end, the frequency of these plus ends decreased with the increasing distance from the cell border (zone 2–5 μm, ▨). Sheet-straight end and blunt-open end were less frequent in zone 0–2 μm (12 and 2%, respectively), nevertheless, in zone 2–5 μm these plus-end conformations were much more prominent (47 and 6%, respectively). The early-frayed, forked, sheet-frayed 1, and blunt-closed conformations were evenly distributed in the two zones. The percentages and absolute numbers are given in Table 2 (Table 2, Supplemental Data).

DISCUSSION

We observed nine predominant types of MT plus-end conformations at the periphery of interphase 3T3s, which we have categorized as early-frayed, frayed, forked, sheet-frayed 1, sheet-frayed 2, sheet-straight, flared, blunt-open, and blunt-closed. We distinguished these types on the basis of their appearance and their kinetic behavior. Most of these plus-end conformations have previously been observed on in vitro–assembled MTs and in situ kMTs, although the nomenclature of plus-end conformations used in different reports is not completely consistent. The sheet-frayed 2 form has, to our knowledge, not been reported until now. Our data indicate that nocodazole causes an increase in frayed plus-end frequency. This finding is in agreement with in vitro studies (Mandelkow and Mandelkow, 1985; Mandelkow *et al.*, 1991; Chrétien *et al.*, 1995; Müller-Reichert *et al.*, 1998; Arnal *et al.*, 2000) and in situ studies on kMTs (VandenBeldt *et al.*, 2006) and indicates that the shrinking MT plus end adopts the frayed conformation. We conclude that interphase MTs at the cell periphery of 3T3 fibroblasts resemble in vitro–assembled and kMTs in many aspects and can be used to understand and interpret the different dynamic states of a MT in situ.

Loss of sheet-straight plus ends upon introduction of nocodazole suggests that these represent the fraction of growing plus ends (Figure 3F). Sheet-straight ends were indeed previously found to be associated with growth in in vitro cryo-EM studies (Chrétien *et al.*, 1995). Sheet-frayed 1 and 2 end frequencies first increased and then decreased upon prolonged nocodazole exposure. The increase could be due to disappearance of the sheet-straight fraction. At the point the sheet-frayed 1 started to decrease, sheet-frayed 2 increased, reaching a peak value at 70 s of exposure (Figure 3, B and C). This indicates that the sheet-frayed 2 end is the stage after the sheet-frayed 1 toward the frayed-end generation (Figure 4).

If we consider the morphology of the sheet-frayed 1 ends, we both find features of MT growth (sheet, GTP-tubulin) and shrinkage (frayed, GDP-tubulin) in this structure. This was also indicated by others (VanBuren *et al.*, 2005), who suggested that these plus ends, having seven of 13 protofilaments GTP-capped, could have growing and shrinking protofilaments at the same time. Once the straight end starts to curve, the extended sheet would shrink more rapidly than the protofilaments at the base of the MT tip, possibly due to the lack of the lateral contacts of the outer layer of protofilaments in the extension. We propose here that the sheet-frayed 1 and 2 conformations are the transition states originating from the sheet-straight rather than from the blunt-open conformation. Our kinetic analysis is supported by the findings of VanBuren *et al.* (2005), who suggested that a sheet-straight end is more likely to collapse/shrink than a blunt-open end. A striking finding from our kinetic analysis is that in a sheet-straight plus-end the protofilaments on the "short" side of the plus end are the first to curve out and depolymerize. Only then do protofilaments on the "extended" side of the plus end start to curve out. An attractive interpretation is that +TIPs are preferentially bound to the extended side of the MT. By maintaining the extended sheet in its straight conformation MTs are "induced" to grow, even when the "short" side of the MT temporarily curves out.

Early-frayed, forked, and blunt-open ends disappear gradually upon nocodazole exposure, whereas the flared end frequency first increases and then decreases during the nocodazole treatment. It is rather difficult to directly deduce from the measured data in Figure 3, which transition paths these ends follow, except that they all eventually transform into the frayed-end. However, by means of kinetic analysis we were able to calculate the rates of probable transformations (Figure 4). Our kinetic analysis suggests that the early-frayed and forked ends both transform into flared ends, which in turn transform into frayed ends. In flared ends the lateral interactions between curving protofilaments are clearly lost, giving rise to further disassembly. In our model a blunt-open end converts into a frayed end. Blunt-open and forked ends both have straight protofilaments, a feature associated with the presence of the GTP-state of tubulin and therefore the growing state of MT (Howard and Timasheff, 1986; Wang and Nogales, 2005; Schek *et al.*, 2007). Given this, in combination with the effect of nocodazole on these conformations, the forked and blunt-open ends could possibly represent growing/stable conformations. For forked ends this was recently suggested by others (Höög *et al.*, 2007). Note that in the latter study the forked end was named and interpreted as "flared."

Interestingly, the early-frayed end has slightly curved protofilaments at the tip. Still it disappears upon prolonged nocodazole treatment (Figure 3E), which indicates that it might represent a stable/growing phase. An explanation might be found in the structural-cap model, described by Janosi *et al.* (2002) in which the protofilaments at the tip of the blunt-open end slightly curve as a result of "relaxation" of the mechanically stressed, though elastic, tube. These ends were suggested to be (meta)stable, pausing ends, which could transition into shrinkage or growth, depending on the circumstances. It is possible that, at least for some

fraction of the found early-frayed ends, this is true. How these ends are generated is not clear to us, as we do not find a transition path between, e.g., blunt-open and early-frayed ends.

Using LM we found ~54% of the plus ends to be growing (i.e., carrying the protein EB1). This value is in the same range as the sum of the fractions of sheet-straight (37%), forked (11%), and blunt-open (5%) ends found in our EM experiments (Figure 1E). These ends might therefore possibly contain structures recognized by EB1. It has been previously suggested that +TIPs might recognize the lumen side of the sheet (Nogales and Wang, 2006). Given the size of GFP-tagged +TIP comets (Perez *et al.*, 1999; Mimori-Kiyosue *et al.*, 2000), this would mean that the lumen of the MT would have to be accessible over a range of a few micrometers. However, we found the maximal sheet length in situ to be 320 nm, which is in the same range as the sheet length reported by others (Austin *et al.*, 2005). It was found that +TIPs exchange very rapidly on MT plus ends in vivo and that this exchange is governed by cytoplasmic diffusion (Dragestein *et al.*, 2008). Together these observations make it unlikely that +TIPs bind the lumen side of MTs.

In close proximity of the cell border (zone <2 μm, Figure 5) sheet-frayed 2, flared, and (early) frayed ends predominate over blunt, forked, sheet-straight, and sheet-frayed 1 ends. Plus-ends associated with shrinkage (i.e., frayed, flared, and sheet-frayed 2) are rather scarce in zone 2–5 μm and plus ends associated with MT growth (sheet-straight, blunt-open) are not as frequent in the area in close proximity of the cell border (zone <2 μm), as they are in the area further away from it. This indicates that the dynamic status of a plus end is influenced by features present in the periphery.

The finding that the ratio of "growth-like" to "shrinkage-like" conformations is ~1.5:1 instead of 2.5:1 (which would be expected at steady state; Komarova *et al.*, 2002; Grigoriev *et al.*, 2006) suggests that a fraction of MTs with a "shrinking" type of conformation might actually not be shrinking, but is instead captured and embedded near the cell membrane by anchoring factors. This, was recently also suggested for the frayed plus ends in kMTs (VandenBeldt *et al.*, 2006). Such stabilization could, for example, be achieved by anchoring of the MT plus end in the cortical actin meshwork. Proteins that are thought to play a role in MT capture mechanisms in the cell periphery include the CLASPs, IQGAP1, and ACF7 (Akhmanova *et al.*, 2001; Fukata *et al.*, 2002; Kodama *et al.*, 2003). With the data reported here, it is not possible to distinguish such stabilized frayed plus ends from the shrinking ones. Nevertheless, the capture of frayed plus ends would explain the shifted ratio of shrinking/growing ends that we found in the periphery of untreated 3T3s.

In conclusion, we have identified nine interchangeable conformations of MT plus ends that are present in the cell periphery of interphase mammalian cells. By combining ET, EM, and LM techniques, we linked MT plus-end conformation to dynamic state. We propose a kinetic model of plus-end transitions from the growing toward the shrinking conformation. Our data indicate that shrinking plus ends might be stabilized by cellular factors associated with the cellular periphery.

ACKNOWLEDGMENTS

We thank Raimond Ravelli and Roman Koning for helpful discussions. This work was supported by the Netherlands Organization for Scientific Research (NWO) and the Dutch Ministry of Economic Affairs (BSIK).

REFERENCES

Akhmanova, A. *et al.* (2001). Clasps are CLIP-115 and -170 associating proteins involved in the regional regulation of microtubule dynamics in motile fibroblasts. Cell. *104*(6), 923–935.

Arnal, I., Karsenti, E., and Hyman, A. A. (2000). Structural transitions at microtubule ends correlate with their dynamic properties in *Xenopus* egg extracts. J. Cell Biol. *149*(4), 767–774.

Austin, J. R., 2nd, Segui-Simarro, J. M., and Staehelin, L. A. (2005). Quantitative analysis of changes in spatial distribution and plus-end geometry of microtubules involved in plant-cell cytokinesis. J. Cell Sci. *118*(Pt 17), 3895–3903.

Caplow, M., and Reid, R. (1985). Directed elongation model for microtubule GTP hydrolysis. Proc. Natl. Acad. Sci. USA *82*(10), 3267–3271.

Caplow, M. (1992). Microtubule dynamics. Curr. Opin. Cell Biol. *4*(1), 58–65.

Caplow, M., Ruhlen, R. L., and Shanks, J. (1994).The free energy for hydrolysis of a microtubule-bound nucleotide triphosphate is near zero: all of the free energy for hydrolysis is stored in the microtubule lattice. J. Cell Biol. *127*(3), 779–788.

Chrétien, D., Fuller, S. D., and Karsenti, E. (1995). Structure of growing microtubule ends: two-dimensional sheets close into tubes at variable rates. J. Cell Biol. *129*(5), 1311–1328.

Dragestein, K. A., van Cappellen, W. A., van Haren, J., Tsibidis, G. D., Akhmanova, A., Knoch, T. A., Grosveld, F., and Galjart, N. (2008). Dynamic behavior of GFP-CLIP-170 reveals fast protein turnover on microtubule plus ends. J. Cell Biol. *180*(4), 729–737.

Fukata, M., Watanabe, T., Noritake, J., Nakagawa, M., Yamaga, M., Kuroda, S., Matsuura, Y., Iwamatsu, A., Perez, F., and Kaibuchi, K. (2002). Rac1 and Cdc42 capture microtubules through IQGAP1 and CLIP-170. Cell *109*(7), 873–885.

Grigoriev, I., Borisy, G., and Vorobjev, I. (2006). Regulation of microtubule dynamics in 3T3 fibroblasts by Rho family GTPases. Cell Motil. Cytoskelet. *63*(1), 29–40.

Höög, J., Schwartz, C., Noon, A., O'Toole, E., Mastronarde, D., McIntosh, J., and Antony, C. (2007). Organization of interphase microtubules in fission yeast analyzed by electron tomography. Dev. Cell *12*, 349–361.

Howard, W. D, and Timasheff, S. N. (1986). GDP state of tubulin: stabilization of double rings. Biochemistry *25*(25), 8292–8300.

Janosi, I. M., Chrétien, D., and Flyvbjerg, H. (2002). Structural microtubule cap: stability, catastrophe, rescue, and third state. Biophys. J. *83*(3), 1317–1330.

Kerssemakers, J. W., Munteanu, E. L., Laan, L., Noetzel, T. L., Janson, M. E., and Dogterom, M. (2006). Assembly dynamics of microtubules at molecular resolution. Nature *442*(7103), 709–712.

Kodama, A., Karakesisoglou, I., Wong, E., Vaezi, A., and Fuchs, E. (2003). ACF7, an essential integrator of microtubule dynamics. Cell. *115*(3), 343–354.

Komarova, Y. A., Akhmanova, A. S., Kojima, S., Galjart, N., and Borisy, G. G. (2002). Cytoplasmic linker proteins promote microtubule rescue in vivo. J. Cell Biol. *159*(4), 589–599.

Kovacs, P., and Csaba, G. (2005). Effect of drugs affecting microtubular assembly on microtubules, phospholipid synthesis and physiological indices (signalling, growth, motility and phagocytosis) in *Tetrahymena pyriformis*. Cell. Biochem. Funct. *24*(5), 419–429.

Krebs, A., Goldie, K. N., and Hoenger, A. (2005). Structural rearrangements in tubulin following microtubule formation. EMBO Rep. *6*(3), 227–232.

Lansbergen, G., and Akhmanova, A. (2006). Microtubule plus end: a hub of cellular activities. Traffic *7*(5), 499–507.

Lieuvin, A., Labbe, J. C., Doree, M., and Job, D. (1994). Intrinsic microtubule stability in interphase cells. J. Cell Biol. *124*(6), 985–996.

Maiato, H., Hergert, P. J., Moutinho-Pereira, S., Dong, Y., VandenBeldt, K. J., Rieder, C. L., and McEwen, B. F. (2006). The ultrastructure of the kinetochore and kinetochore fiber in *Drosophila* somatic cells. Chromosoma *115*(6), 469–480.

Mandelkow, E. and Mandelkow, E. R. (1985). Unstained microtubules studied by cryo-electron microscopy. Substructure, supertwist and disassembly. J. Mol. Biol. *181*(1),123–135.

Mandelkow, E. M., Mandelkow, E. and Milligan, R. A. (1991). Microtubule dynamics and microtubule caps: a time-resolved cryo-electron microscopy study. J. Cell Biol. *114*(5), 977–991.

Mimori-Kiyosue, Y., Shiina, N. and Tsukita, S. (2000). The dynamic behavior of the APC-binding protein EB1 on the distal ends of microtubules. Curr. Biol. *10*(14), 865–868.

Mitchison, T., and Kirschner, M. (1984). Microtubule assembly nucleated by isolated centrosomes. Nature *312*(5991), 232–237.

Mitchison, T. J., (1993). Localization of an exchangeable GTP binding site at the plus end of microtubules. Science *261*, 1044–1047.

Muller-Reichert, T., Chretien, D., Severin, F., and Hyman, A. A. (1998). Structural changes at microtubule ends accompanying GTP hydrolysis: Information from a slowly hydrolyzable analogue of GTP, guanylyl (alpha, beta) methylenediphosphonate. Proc. Natl. Acad. Sci. USA *95*, 3661–3666.

Nogales, E., and Wang, H. W. (2006). Structural intermediates in microtubule assembly and disassembly: how and why? Curr. Opin. Cell Biol. *18*(2), 179–184.

O'Toole, E. T., McDonald, K. L., Mantler, J., McIntosh, J. R., Hyman, A. A., and Muller-Reichert, T. (2003). Morphologically distinct microtubule ends in the mitotic centrosome of *Caenorhabditis elegans*. J. Cell Biol. *163*(3), 451–456.

Perez, F., Diamantopoulos, G. S., Stalder, R., and Kreis, T. E. (1999). CLIP-170 highlights growing microtubule ends in vivo. Cell *96*(4), 517–527.

Ravelli, R.B.G., Gigant, B., Curmi, P. A., Jourdain, I., Lachkar, S., Sobel, A., and Knossow, M. (2004). Insight into tubulin regulation from a complex with colchicine and a stathmin-like domain. Nature *428*, 198–202.

Ress, D., Harlow, M. L., Schwarz, M., Marshall, R. M., and McMahan, U. J. (1999). Automatic acquisition of fiducial markers and alignment of images in tilt series for electron tomography. J. Electron. Microsc. *48*(3), 277–287.

Saoudi, Y., Fotedar, R., Abrieu, A., Doree, M., Wehland, J., Margolis, R. L., and Job, D. (1998). Stepwise reconstitution of interphase microtubule dynamics in permeabilized cells and comparison to dynamic mechanisms in intact cells. J. Cell Biol. *142*(6), 1519–1532.

Schek, H. T., 3rd, Gardner, M. K., Cheng, J., Odde, D. J., and Hunt, A. J. (2007). Microtubule assembly dynamics at the nanoscale. Curr. Biol. *17*(17), 1445–1455.

Schuyler, S. C., and Pellman, D. (2001). Microtubule "plus-end-tracking proteins": the end is just the beginning. Cell *105*, 421–424.

Stepanova, T., Slemmer, J., Hoogenraad, C. C, Lansbergen, G., Dortland, B., De Zeeuw, C. I., Grosveld, F., van Cappellen, G., Akhmanova, A., and Galjart, N. (2003). Visualization of microtubule growth in cultured neurons via the use of EB3-GFP (end-binding protein 3-green fluorescent protein). J. Neurosci. *23*(7), 2655–2664.

Tran, P. T., Walker, R. A., and Salmon, E. D. (1997). A metastable intermediate state of microtubule dynamic instability that differs significantly between plus and minus ends. J. Cell Biol. *138*, 105–117.

VanBuren, V., Cassimeris, L., and Odde, D. J. (2005). Mechanochemical model of microtubule structure and self-assembly kinetics. Biophys J. *89*(5), 2911–2926.

VandenBeldt, K. J., Barnard, R. M., Hergert, P. J., Meng, X., Maiato, H., and McEwen, B. F. (2006). Kinetochores use a novel mechanism for coordinating the dynamics of individual microtubules. Curr. Biol. *16*(12), 1217–1223.

Vorobjev, I. A., Alieva, I. B., Grigoriev, I. S., and Borisy, G. G. (2003). Microtubule dynamics in living cells: direct analysis in the internal cytoplasm. Cell Biol. Int. *3*, 293–294.

Wade, R. H., and Chrétien, D. (1993). Cryoelectron microscopy of microtubules. J. of Struct. Biol. *110*, 1–27.

Wang, H. W., and Nogales, E. (2005). Nucleotide-dependent bending flexibility of tubulin regulates microtubule assembly. Nature *435*, 911–915.